Superconducting characteristics and microstructure of polycrystalline Zn-doped In_2O_3 films

Shinozaki, Bunju
Department of Physics, Kyushu University

Takada, Satoshi
Department of Physics, Kyushu University

Kokubo, Nobuhito
Center for Research and Advancement in Higher Education, Kyushu University

Makise, Kazumasa
High Voltage Electron Microscopy Station, National Institute for Material Science

他

出版情報：Physica C : Superconductivity and its Applications. 471 (21/22), pp.717-720, 2011-11. Elsevier B.V.
バージョン：

SUPERCONDUCTING CHRACTERISTICS AND MICROSTRUCUTRE OF POLYCRYSTALLINE Zn-DOPED In_2O_3 FILMS

B. Shinozaki[1*], S.Takada[1], N.Kokubo[2], K. Makise[3*], K. Mitsuishi[3], K.Yamada[1], K. Yano[4], H. Nakamura[4]

[1] Department of Physics, Kyushu University, Fukuoka 812-8581, Japan

[2] Center for Research and Advancement in Higher Education, Kyushu University, Fukuoka 819-0395, Japan

[3] High Voltage Electron Microscopy Station, National Institute for Material Science, 3-13 Sakura, Tsukuba, Ibaraki 305-0003, Japan

[4] Advanced Technology Research Laboratories, Idemitsu Kosan Co. Ltd., Chiba, 299-0293, Japan

In order to investigate the relation among the superconducting transition T_c, carrier density n, resistivity ρ and the microstructure in the Polycrystalline $(In_2O_3)_{1-x}$-$(ZnO)_x$ films, we prepared specimen films by post annealing of amorphous films with x=0.025 at various annealing temperature T_a and for annealing time t_a=1 h and 4 h. As for microstructures, we have investigated the distribution of elements by scanning transmission electron microscopy (STEM) and electron energy-loss spectroscopy (EELS). We have found followings: 1) The annealed films clearly show the superconductivity of which T_c depends on T_a, t_a and n. This indicates that the superconductivity is determined by the combination of crystallinity and carrier density. 2) The data on STEM-EELS spectra mapping of indium plasmon indicate that droplets of the pure indium phase exist inside a film, where the distribution of these droplets dispersed. Therefore, it seems that droplets do not form an electrical conducting path, that is, it is possible that observed superconductivity is due to intrinsic characteristic of polycrystalline $(In_2O_3)_{1-x}$-$(ZnO)_x$ films.

PACS 75.15.Rn, 74.62.-c,74.78.Db

Key word; annealing effect, EELS, low carrier superconductivity

* Present address: Kobe advanced ICT research center, National Institute of information and communications Technology, 588-2 Iwaoka Kobe Hyogo 651-2492 Japan

*Corresponding Author

Bunju Shinozaki

Tel and Fax; 81-92-642-3895

E-mail address; shinozaki@phys.kyushu-u.ac.jp

1. Introduction

As for a transparent electrode material for devices such as liquid crystal displays, amorphous zinc-doped indium oxide(a-In_2O_3-ZnO) have practically attracted considerable interest. These films can give a smooth surface to enable fine processing with a high accuracy and have large values of Hall mobility μ. [1-3] On the other hand, investigations of the fundamental electrical properties of a-In_2O_3-ZnO are very interesting from the viewpoint of quantum corrections in dirty systems because the resistivity and carrier density n of this material are easily changed by film preparation method and/or post annealing conditions.

For annealing effects on the electrical resistivity ρ, investigations at room temperature have been extensively done.[4,5] However, detailed investigations at low temperatures of the transport properties in polycrystalline In_2O_3-ZnO films are few.

Recently, we have observed that the $(In_2O_3)_{1-x}$-$(ZnO)_x$ films annealed at 200℃ in atmosphere show the behavior indicating the superconducting phenomenon under the restricted condition of $x \leq 0.02$, although n is small as $n \approx 10^{26}/\mathrm{m}^3$.[6] The estimated n is less than that of other In oxide systems showing the superconductivity.[7,8] On the other hand, for annealed indium-tin oxide films(ITO), it has been already reported that analyses by technique of electron-energy-loss spectroscopy (EELS) and energy-dispersive X ray spectroscopy show the segregation of tin near the boundary or the existence of pure indium particles.[9-11] These results give a question that the superconductivity observed in doped indium oxide films such as present specimens is intrinsic phenomenon or not.

In this work, we report that polycrystalline In_2O_3-ZnO films prepared by restricted annealing conditions in air show superconductivity. In order to clarify the segregation of indium of present annealed In_2O_3-ZnO films affect the occurrence of superconductivity or not, we have analyzed the distribution of indium by EELS observation.

2. Film preparation and Experimental procedure

Firstly, amorphous In_2O_3-ZnO films with 350 nm thick were prepared by deposition on glass substrates by the DC-magnetron sputtering method under 0.3 Pa of argon using the ceramic oxide $(In_2O_3)_{1-x}$-$(ZnO)_x$ target with varying x. During deposition, the substrate temperature was kept at room temperature. From the results of X-ray diffraction (XRD), it is recognized that as-deposited films have an amorphous structure.

We annealed the amorphous films in air on a hot plate preheated to an annealing temperature T_a between 200℃ and 300℃. To investigate the effects of annealing time t_a on

transport properties and film structures, we changed t_a from 0.5 to 20 h at T_a=200℃for films with x=0.01. As shown in previous report [12], these films show the systematic changes of T_c and diffraction intensity depending on t_a; both the diffraction intensity and T_c monotonically increase with increase of t_a. In this series, the carrier n takes values in a range of $\approx 4\times10^{25}/\mathrm{m}^3 < n < 3\times10^{26}/\mathrm{m}^3$. In the present work, we prepared polycrystalline films with $x = 0.025$ by annealing at various values of T_a between 200℃and 300℃keeping t_a as 1h and 4h. By this procedure, we obtained the films of which n is in the range of $\approx 1\times10^{25}/\mathrm{m}^3 < n < 3\times10^{26}/\mathrm{m}^3$.

We measured the temperature dependence of resistivity ρ and Hall coefficient R_H, using a standard dc four-probe technique in the temperature range from 0.5 K to 300 K. The determination of temperature was made to an accuracy of about 10^{-3} K. For R_H, we applied a magnetic field of H=± 5 T perpendicular to the film surface. We confirmed that a linear characteristic of Hall resistance holds in the magnetic field region -5 T≤ H ≤ 5 T. The detailed procedure has been given in the previous work. [13]

3. Experimental results and Discussions

First, we show the structure of the film with x=0.01 annealed for t_a = 20 h. Figure 1 shows the HAADF-STEM (High-Angle-Annular-Dark-Field Scanning-Transmission-Electron-Microscope) image for low-loss EELS(Electron Energy-Loss Spectroscopy) spectra. We can find a grain boundary at the center in the image, where the right part is only a little dark. Further, we recognize the existence of scattered white or black spots. It is possible that these regions are made by different elements and/or have different thickness from other region. In order to obtain further information in the region of center part enclosed by the square in Fig.1, we measured low-loss EELS spectra, which can provide useful information on the interactions between the incident electron beam and the solid. Details are given in the reports by Tanaka[14] and Furuya [15]. The loss energy range from 0 to 70 eV of the spectrum includes much information about zero loss, elastic scattering and the plasmon.[16]

Figure 2(a) shows a map of indium plasmon obtained by STEM-EELS spectra mapping for the same square region in Fig.1. We can clearly see some distinct white-regions, marked by arrow b of which diameter of around $10-20$ nm. The detailed fitting procedure is shown in Ref. 16. To remove the influence of an erroneous background in the fitting procedure, we performed a MLLS (multiple linear least-squares) fit to the indium plasmon, using the

spectra for the InO phase and pure indium as references. Figures 2(b) and 2(c) show the low-loss EELS spectra taken in the region denoted by the arrow b and in the other region arrowed by c, respectively. The spectrum in Fig.2(b) shows the peak at 11.4 eV corresponding to the bulk plasmon peak for pure indium. This spectrum indicates the possibility that these regions include pure indium.

Figure 2(a), however, clearly shows that the spots (indium droplets) completely are isolated. Therefore, these droplets do not seem to form continuous electrical-conducting paths because of scattered distribution of droplets. This means that it is possible that observed superconducting transition discussed below comes from intrinsic characteristic of polycrystalline $(In_2O_3)_{1-x}$-$(ZnO)_x$ films but not due to the aggregation of indium droplets.

In order to clarify the annealing effect on superconductivity, we start to show the T_a dependence of n and ρ. Figure 3(a) shows the T_a dependence of n, where the value n of the as-deposited amorphous film is $6.3\times10^{26}/\mathrm{m}^3$. Bellow T_a<300℃, we can control n in a wide range between $\approx 6\times10^{26}/\mathrm{m}^3$ and $0.1\times10^{26}/\mathrm{m}^3$. Although n of films annealed for 4 h seems to decrease monotonically, n for 1 h films takes a dip around T_a=230℃. In Fig.3(b), we show n dependence of ρ. The solid line shows the relation of $\rho \propto 1/n$ determined to fit the data in the low resistivity region. However, the data deviate from this relation in the region below $n^* \approx 0.4\times10^{26}/\mathrm{m}^3$. It is probable that the origin of the deviation is due to the increment of inter-grain resistivity. As shown in the inset, there is a difference of the T_a dependence of ρ between data for t_a=1 h and t_a=4 h, while there is no remarkable difference in $\rho - n$ relation for both films. As for an effect of crystallinity on superconductivity, we will discuss along the Figure 4 in next paragraph.

For the films annealed for 1 h, we can find that the superconducting behavior appears in the films annealed in a range of $\approx 220℃ \leq T_a < \approx 280$ ℃. Figure 4(a) shows the typical temperature dependence of the resistivity of film annealed at T_a=230℃for 1 h. The superconducting transition temperature T_c was defined as a temperature at which half of the normal state resistance was restored. On the other hand, for films annealed for 4 h, the maximum T_a bringing superconductivity may be below 260℃. In the previous report for the films with $x = 0.01$ annealed at 200℃ for different annealing times[6], we have shown that the magnitude of T_c strongly correlates with the crystallinity. If we assume that the T_c of films with $x = 0.025$ depends on the crystallinity determined by annealing temperature T_a, we expect that the T_c of films annealed for 4 h film is higher than that of films for 1 h. However, the values of T_c for 4 h are lower than that for 1 h. On the other

hand, as shown in Fig.4(b), it seems that the transition temperature T_c shows good correlation with n compared with T_a. This indicates that the appearance of superconductivity of the present system does not determined only by crystallinity but the combination of crystallinity and the carrier density.

3. Conclusion

For polycrystalline $(In_2O_3)_{1-x}$-$(ZnO)_x$ films annealed in air, we have investigated the microstructure and the transport properties. From the detailed analysis of EELS observation, the distribution of indium droplets was found to be scattered. It is unlikely that these droplets form the electrical conducting path in annealed films. Therefore, we consider that the superconductivity in our polycrystalline In_2O_3-ZnO films cannot be assigned to continuous metallic indium channels. We have observed the resistive transition indicating superconductivity at low temperatures below 2.8 K for films with $x = 0.025$ annealed at temperatures between 200℃ and 300℃ for annealing time t_a 1 h and 4 h. Although data in the T_c - T_a relation are scattered depending on t_a, the T_c shows relatively good correlation with n taking convex form.

References

[1] T. Minami, T. Kasumu, S. Takata, J. Vac. Sci. Technol. A 14 (1996) 1704.

[2] Y.S. Jung, J.Y. Seo, D.W. Lee, D.Y. Jeon, Thin Solid Films 445 (2003) 63.

[3] N. Ito, Y. Sato, P.K. Song, A. Kaijo, K. Inoue, Y. Shigesato, Thin Solid Films 496 (2006) 99.

[4] J.R. Bellingham, W. A. Phillips, C. J. Adkins, J. Phys.:Condens. Mat. 2 (1990) 6207.

[5] H. Nakazawa, Y. Ito, E. Matsumoto, K. Adachi, N. Aoki, Y. Ochiai, J. Appl. Phys. 100 (2006) 093706.

[6] B. Shinozaki, N. Kokubo, K. Makise, S. Takada, T. Yamaguti, S. Ogura, K. Yamada, K. Yano, K. Terai, S. Tomai, H. Nakamura, Physica C 469 (2009) 956.

[7] N. Mori, J. Appl. Phys. 73 (1993) 1327.

[8] D. Kowal, Z. Ovadyahu, Physica C 4 (2008) 322.

[9]K.A. Mkhoyan, T. Babinec, S.E. Maccagnano, E.J. Kirkland, J. Silcox, Ultramicroscopy 107 (2007) 345.

[10]P. Harkins, M. MacKenzie, A.J. Crave, D.W. MacComb, Micron 39 (2008) 709.

[11] H. Morikawa, H. Kurata, M. Fujita, J. Electron Microsc. 49 (2000) 67.

[12] B. Shinozaki, N. Kokubo, S. Takada, K. Yamada, K. Makise, K. Inoue, H. Nakamura, J.Phys. Conf. Ser. 150 (2009) 052234.

[13] B. Shinozaki, K. Makise, Y. Shimane, H. Nakamura, K. Inoue, J. Phys. Soc. Jpn. 76 (2007) 074718.

[14] N. Tanaka, Sci. Technol. Adv. Mater. 9 (2008) 014111.

[15] K. Furuya, Sci. Technol. Adv. Mater. 9 (2008) 014110.

[16] K. Makise, K. Mistuishi, N. Kokubo, T. Yamaguti, B. Shinozaki, K. Yano, K. Inoue, H. Nakamura, J.Appl.Phys.108 (2010) 023704.

Figure captions

Fig.1 HAADF-STEM image for low-loss EELS spectra of a film with x=0.01 annealed at 200℃. The square marked by the Spectrum image is the area analyzed by the low-loss EELS in Fig.2(a). The arrows b and c in the square show the regions corresponding to that analyzed by EELS spectra shown in Figs.2(b) and 2(c).

Fig.2 (a) A map of indium plasmon obtained by STEM EELS spectra mapping in the region enclosed by the square in Fig.1. (b) Spectrum taken at the region denoted by the arrow b in Fig.1 and Fig.2(a). The peak at 11.4 eV marked by the arrow ↓ corresponds to that in the pure indium. (c) Spectrum taken in the region denoted by the arrow c in Fig.1 and Fig.2(a).

Fig.3 (a) T_a dependence of n determined by the Hall coefficient measurement. (○) films annealed for 1 h. (●) films annealed for 4 h. (b) n dependence of ρ at 300 K. The solid line shows the relation of $\rho \propto 1/n$. The inset shows the T_a dependence of ρ.

Fig.4 (a) T dependence of ρ of the annealed film at T_a=230℃ for 1 h for a wide temperature region. The inset shows the ρ -T relation at low temperatures near T_c. (b) The carrier density n dependence of T_c for both films annealed for 1 h and 4 h at various T_a.

Figure 1

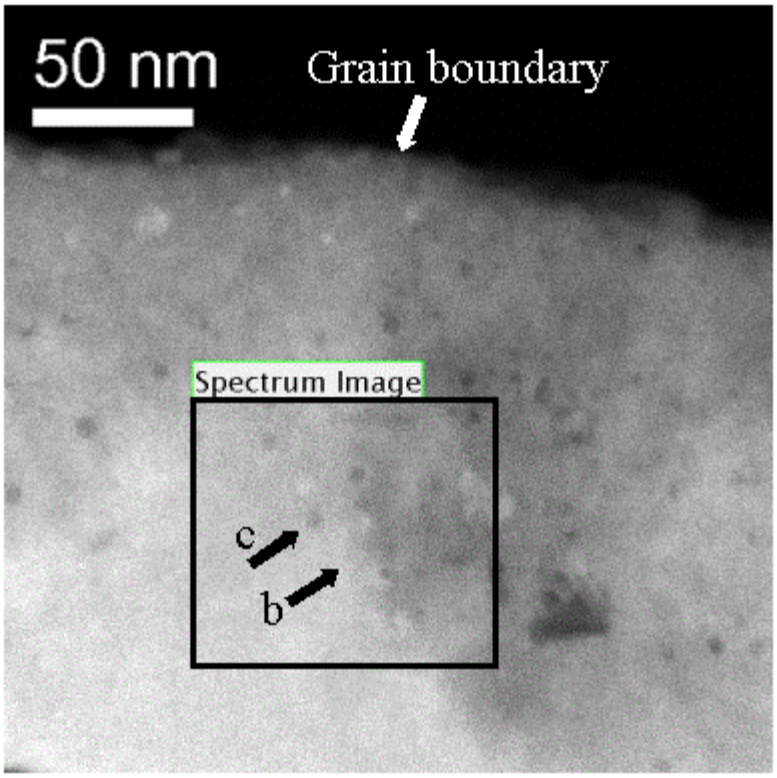

Fig. 2 (a)

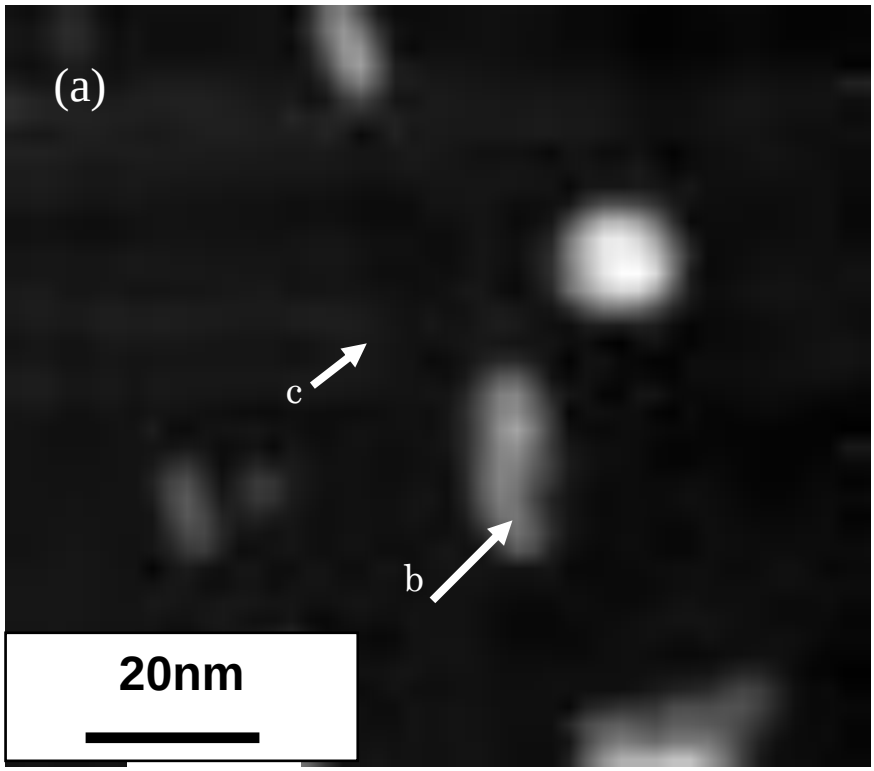

Fig.2(b) (c)

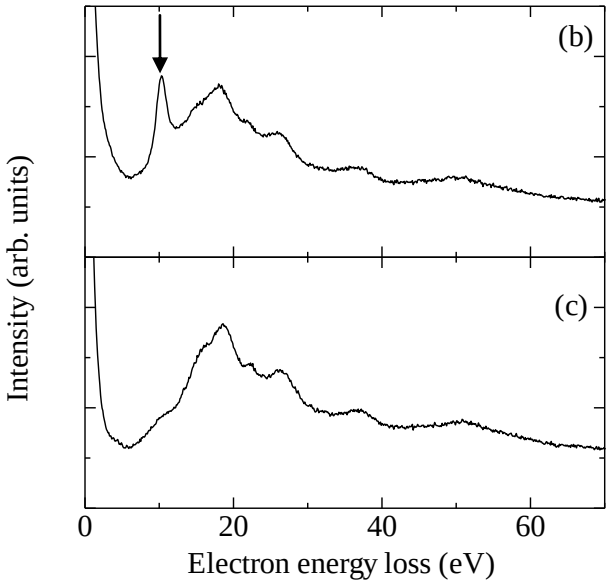

Fig.3(a)

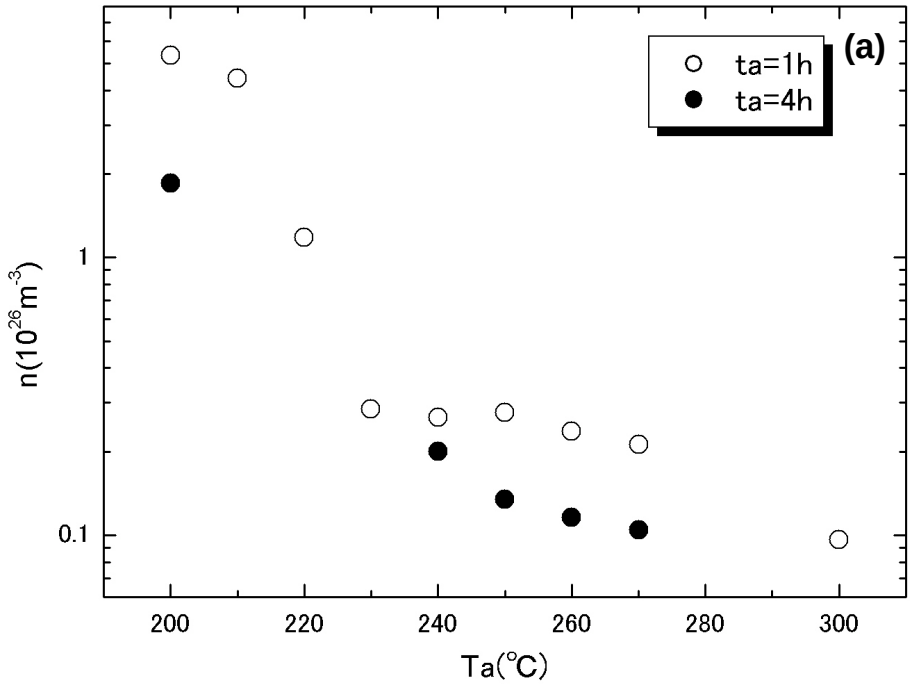

Fig.3(b)

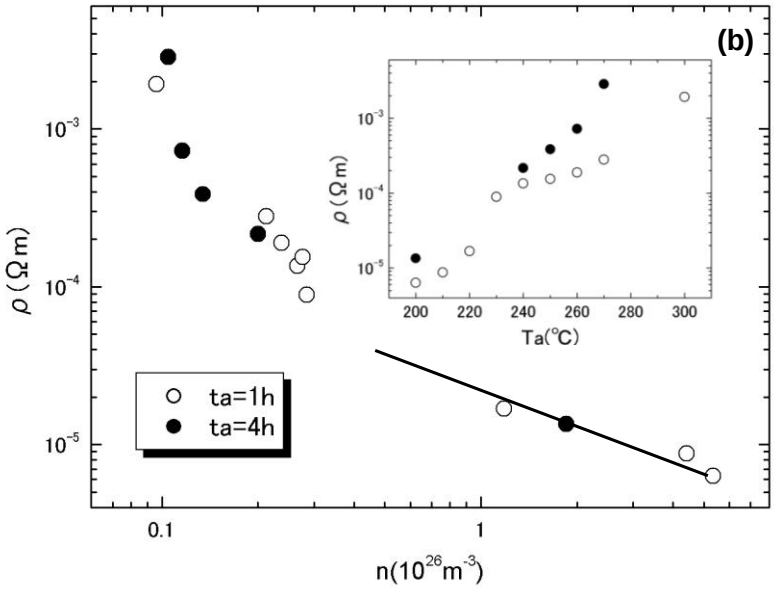

Fig.4(a)

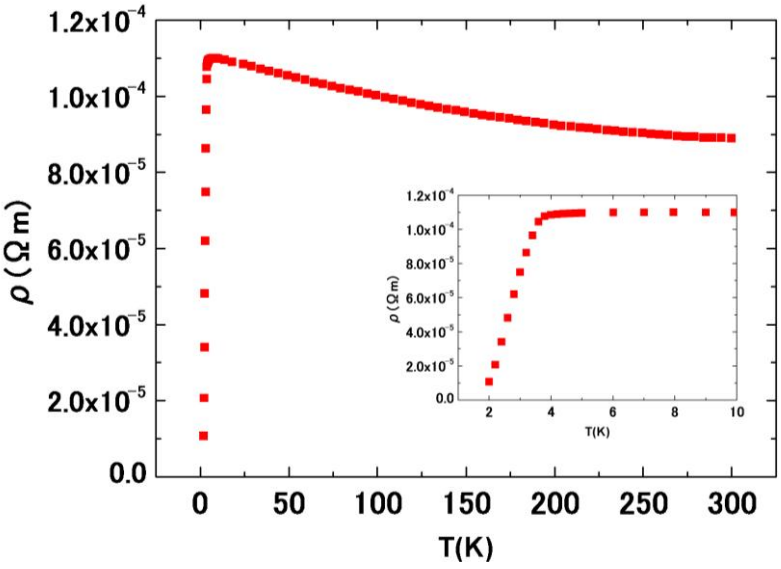

Fig.4(b)

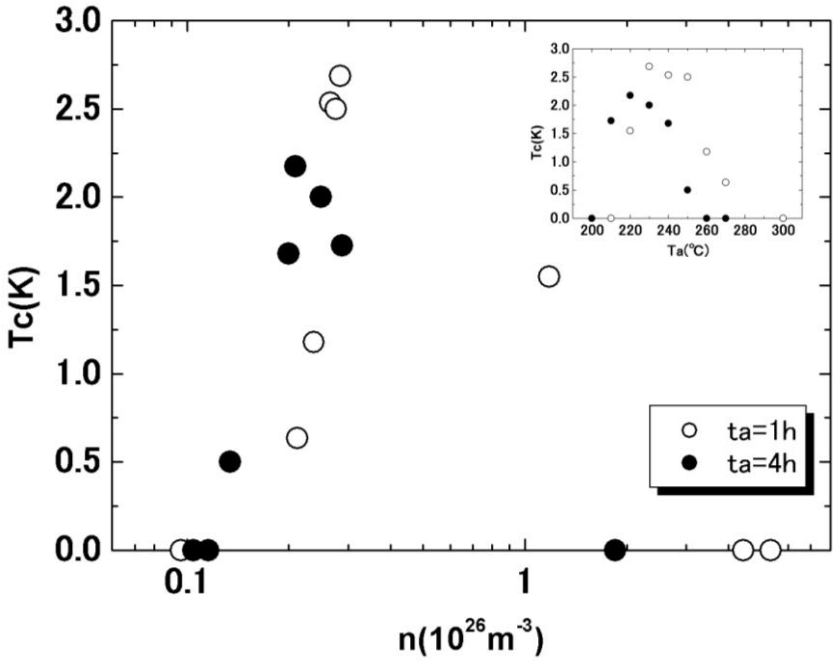
3.0
2.5
2.0
1.5
1.0
0.5
0.0
Tc(K)
0.1
1
n(10^26 m^-3)
ta=1h
ta=4h
Tc(K)
Ta(℃)
200
220
240
260
280
300